

Effect of Intake Charge Temperature on Oxy-Fuel Combustion (OFC) in an HCCI Diesel Engine under Different CO₂ Dilutions

Raouf Mobasheri ^{a, b, *}, Abdel Aitouche ^{a, b}, J. B. Mumputu ^b, Xiang Li ^c, Zhijun Peng ^d

^a Univ. Lille, CNRS, Centrale Lille, UMR 9189 - CRISTAL - Centre de Recherche en Informatique
Signal et Automatique de Lille, F-59000 Lille, France

^b Junia, Smart Systems and Energies, F-59000 Lille, France

^c School of Computer Science and Technology, University of Bedfordshire, Luton, UK

^d School of Engineering, University of Lincoln, Lincoln, UK

* Corresponding author:

Raouf Mobasheri, Associate Professor of Mechanical Engineering

Department of Smart Systems and Energies

JUNIA – HEI School of Advanced Engineering Studies

13 Rue De Toul, BP41290 59014 Lille Cedex, France

E-mail: raouf.mobasheri@junia.com, Phone: +33 (0)3 28 38 48 58

Abstract

Carbon dioxide is one of the leading contributors to global warming. Oxy-fuel combustion (OFC) integrated with Carbon Capture and Storage (CCS) technology is an efficient way to reduce carbon dioxide emissions. In OFC, pure oxygen (O₂) is used instead of air to react with hydrocarbon fuel. Consequently, the products of combustion mainly include carbon dioxide (CO₂) and water vapor (H₂O) under lean conditions. Meanwhile, due to the absence of N₂ in the intake charge, nitrogen-related emissions such as NO_x are greatly removed from the exhaust gases. In the present study, the effect of intake charge

22 temperature on OFC has been investigated in a diesel engine under the Homogeneous Charge
23 Compression Ignition (HCCI) mode. In order to control combustion temperature and avoid overheating
24 problems caused by oxygen in OFC, a portion of the exhaust CO₂ was added to the O₂. For this purpose,
25 different CO₂ dilutions ranging from 79-85% have been employed. It has been found that OFC can
26 significantly reduce CO and PM emissions while eliminating NO_x emissions. With a higher intake charge
27 temperature, combustion occurs earlier with shorter main stages, reducing the Indicated Mean Effective
28 Pressure (IMEP) and increasing the Indicated Specific Fuel Consumption (ISFC), whereas, with a lower
29 intake charge temperature, combustion stability deteriorates leading to incomplete OFC. By raising the
30 intake charge temperature from 140°C to 220°C and applying 21% O₂ and 79% CO₂ v/v, the Indicated
31 Thermal Efficiency (ITE) is reduced from 34.6% to 29.2% while ISFC is increased from 0.24 to 0.285
32 Kg/kWh.

33 **1. Introduction**

34 Global warming due to greenhouse gases (GHG) is a growing concern worldwide [1]. All countries face
35 global climate change, a major challenge affecting human survival and development [2-4]. GHGs have
36 long-term effects on global climate change, which has a variety of environmental impacts. CO₂ is one of
37 the leading causes of global warming [5-6]. The primary source of CO₂ is the burning of fossil fuels to
38 generate energy. Further development of low-carbon technologies can improve energy efficiency, reduce
39 reliance on fossil fuels, and prevent the rapid growth of CO₂ and other greenhouse gases [7]. Over the years,
40 the interest in developing new techniques that result in reducing the emissions of primary long-lasting GHG
41 carbon dioxide (CO₂) has considerably arisen among scientists and engineers. For conventional internal
42 combustion engines (ICEs), oxy-fuel combustion (OFC) and carbon capture and storage (CCS) techniques
43 are considered to offer great potential [8-10]. Currently, the OFC technology is mostly applied in the
44 thermal power generation industry focused on the coal power plant [11-13], biomass-fired power plants

45 [14], and high-velocity oxy-fuel coating processes [15]. In addition, its utilization is assessed as being
46 employed for the refining sector [16].

47 The European Union (EU) has reported that the transportation sector is responsible for about 28% of the
48 total CO₂ emissions, while road transport is subject for more than 70% of the total emissions of the
49 transportation sector [17]. The majority of GHG emissions of the transportation sector come from burning
50 fossil fuels for cars, trucks, trains, ships, and planes [18]. Approximately 90% of transportation fuel is
51 petroleum, mostly gasoline and diesel [19]. The combustion of petroleum-based products leads to CO₂
52 emissions. EU regulations have imposed limits on carbon emissions and certification of internal
53 combustion engines for non-road mobile machinery. As a result, the inland waterways (IW) vessels must
54 meet the prescribed emission standards [20].

55 Many research has emerged to improve the overall performance and fuel economy of conventional engines
56 to meet the demands of a clean and efficient diesel engine [21]. Innovative technologies, such as alternative
57 solar power, hybrid electricity, plug-in hybrid power, and battery power, are reducing diesel engines' carbon
58 emissions. Nevertheless, these technologies are too expensive and their output torque is low to be widely
59 applied to heavy-duty engines used in waterway transportation. [22-23].

60 Besides the application of the OFC technology to other sectors, such as coal-fired power generation [24-
61 25], it has been of interest to use it in ICEs. The application of OFC in ICEs was studied by Osman, in 2009
62 [26]. In this study, a water injection system was applied to control the in-cylinder temperature. The results
63 showed that heated water absorbs combustion heat and becomes vapor once it is inside the combustion
64 chamber. In the vapor state, it will enhance the gas expansion during the expansion stroke. Additionally,
65 heated water and fuel oxidation complement one another and produce a high work output. Recently, a
66 number of studies have been conducted on OFC, including Kang et al. [27], who demonstrated that OFC
67 technology can be used in a homogeneous charge compression ignition engine (HCCI) in order to reduce
68 complexity in engine emissions after-treatment techniques and reduction of pollutant emission. In their test

69 bench, they simulated exhaust gas recirculation by using an oxygen and carbon dioxide mixture intake
70 system with variable oxygen fraction adjustment capability. Their results showed that the high-temperature
71 and high-pressure water injected into the combustion chamber with an appropriate injection strategy
72 controls the abnormal combustion and helps to increase the thermal efficiency of the system. Li et al. [28]
73 demonstrated numerically the use of OFC on a practical diesel engine at the economical oxygen-fuel ratios.
74 In their study, a 1D simulation analysis of the influence of various operating parameters on engine power
75 recovery was considered. They concluded that, within a certain range, a decrease in the intake temperature
76 or the CO₂ ratio could lead to a recovery in engine power. In addition, the increase of λ_{O_2} from 1.0
77 to 1.5, which is chosen as the final solution due to improvements in oxygen consumption, can significantly
78 improve engine power from 33.5kW to 40kW, even though other operating parameters remain unchanged.
79 Xiao Yu et al. [29] studied the combustion characteristics of a quasi ICRC on a single-cylinder SI engine
80 fueled with propane. In their research, a gas mixture of O₂-CO₂ has been used to simulate EGR to control
81 the temperature in the cylinder. They considered water injection into the cylinder near the top dead center
82 in order to control the OFC process. Their results revealed that a quasi ICRC cycle was established on a
83 reciprocating engine by injecting overheated water into the cylinder near the top dead center in an oxy-fuel
84 combustion process and resulting in the enhancement of the cycle performance. In addition, they reported
85 that the evaporation of injected water increases the working gas near the top dead center and extends the
86 isobaric expansion process. Based on their results, they report an 8.4% increase in the indicated work. As
87 the literature indicates, the use of OFC makes it possible to completely reduce the expensive NO_x after-
88 treatment systems. It is also fuel-efficient and has low levels of particulate emissions [30]. This paper
89 discusses the effect of intake charge temperature (in a range of 140°C to 220°C) on OFC in an HCCI diesel
90 engine under different diluent strategies. The HCCI mode has been used due to its high thermal efficiency
91 and ultra-low NO_x and particulate matter (PM) emissions [31].

92 **2. Integrated concept of the RIVER project**

93 The current study has been done as a part of an EU-Funded project called RIVER (funded by Interreg
94 North-West Europe) [20]. The purpose of the RIVER project is to apply OFC technology accompanied by
95 CCS techniques to develop possible solutions to eliminate NOx emissions from inland boat engines as well
96 as to capture and store carbon emissions from these engines.

97 Figure 1 shows a schematic view of OFC technology proposed by RIVER project. As shown in Figure 1,
98 the boat utilizes a diesel-generator as its power system. According to RIVER's technology, O₂ is supplied
99 via a high-pressure oxygen tank. The flue gas stream, which mainly contains CO₂-rich combustion gases,
100 is condensed in a condenser with connected water separation. During the OFC working conditions, some
101 part of the CO₂ is returned to the cylinder, pre-mixed with O₂ in a chamber for being fed into the engine.
102 The remaining CO₂ is then compressed and stored in the storage tank. The implementation of this
103 technology will be of great value to the removal of NOx emissions while storing all carbon dioxide.

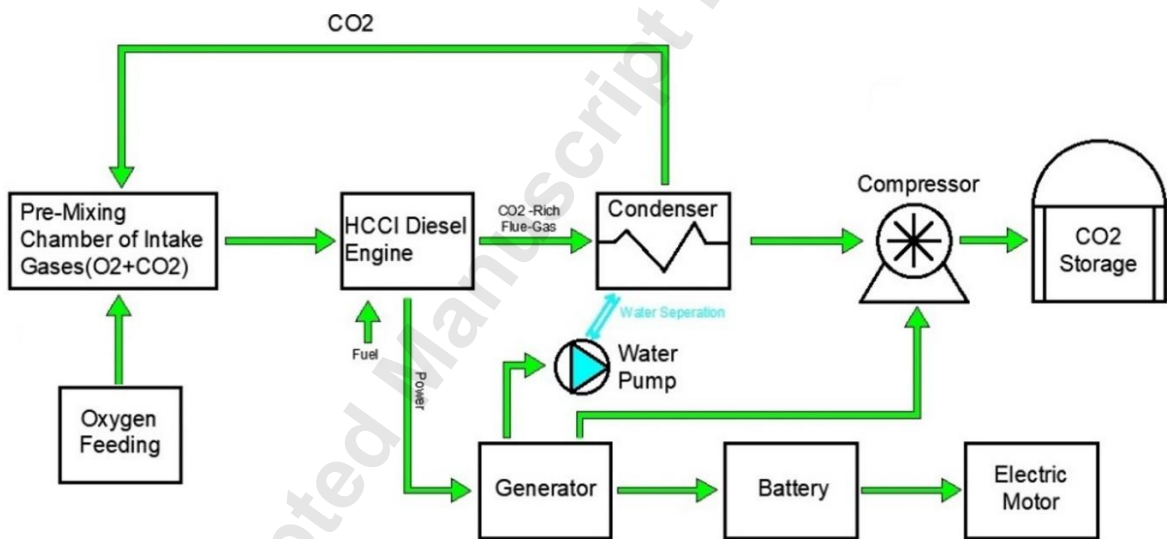


Figure 1. Schematic view of OFC technology proposed by RIVER project

106 The proposed idea of using OFC has a significant advantage over previous studies in that the diluent
107 strategy is integrated with HCCI combustion to control the OFC process instead of direct in-cylinder water
108 injection, meanwhile, it can eliminate problems associated with water injection such as lubrication and
109 corrosion [26].

Downloaded from <http://asmedigitalcollection.asme.org/gasturbinespower/article-pdf/doi/10.1115/1.4055882/6924323/gtp-22-1149.pdf> by University of Lincoln user on 08 October 2022

110 3. Numerical study

111 A commercial CFD package AVL Fire code was used to perform the CFD simulation [32]. A reduced
112 chemical mechanism with 349 reactions and 76 species [33] was applied to simulate the combustion process
113 and emission under the HCCI combustion and OFC technology. The authors have already applied this
114 mechanism for simulating various combustion regimes and have achieved good agreement when modeling
115 combustion and emissions [33-36].

116 Table 1 summarizes all computational models used for CFD simulations. In addition, Table 2 shows the
117 setting for the KHRT breakup model parameter applied to the simulation.

118 Table 1. Applied computational models

Combustion and emissions	Reduced chemical n-heptane-n-butanol-PAH mechanism (349 reactions and 76 species)
Turbulence	K-zeta-f model
Primary breakup	Blob Injection model
Breakup	KHRT model
Evaporation	Dukowicz model
Particle interaction	Schmidt model
Drag law	Schiller Naumann
Wall interaction	Walljet1

119
120 Table 2. The parameters set up for the KHRT breakup model

Model constants	Value
KH-WAVE to adjust the stable radius of droplets (C1)	0.61
KH-WAVE used to adjust the break-up time (C2)	12
Type constant to adjust break-up length (C3)	10
RT model constant used to adjust wavelength (C4)	5.33
RT model constant used to adjust break-up time (C5)	1
Constant for child droplet parcel number adjustment (C6)	0.3
Constant for child droplet parcel mass adjustment (C7)	0.05
Constant to adjust droplet normal velocity (C8)	0.188

121
122 The engine specifications are listed in Table 3. The experiment was carried out on a single cylinder of this
123 engine at 1500 rev/min and 6.8 bar IMEP (Indicated Mean Effective Pressure) [21].

124 Table 3. Engine Specification

Engine name	Ford Puma DuraTorq
Type	4 Cylinder, 4 stroke diesel engine
Combustion chamber	Bowl in piston
Valves per cylinder	4
Bore [mm] × stroke [mm]	86 × 86
Squish Height [mm]	0.86
Comperation ratio	18.2:1
Displacement [cm ³]	1998
IVC [BTDC]	143°
IVO [ATDC]	335°
EVC [BTDC]	355°
EVO [ATDC]	131°
Swirl ratio @ IVC	1.1
Connecting rod length [mm]	155
Peak cylinder pressure [MPa]	18
Injection system	Common rail DI [up to 180 MPa]
Injector	Solenoid with 6 holes
Injector hole diameter [mm]	0.159
Injection angle	154°
Diesel injection pressure[MPa]	150
Number of injection [/cycle]	4
Diesel SOI [°CA]	@ 306, 314, 326, 338
Injection Duration [μs/injection]	230

125

126 The CFD calculations was performed on a 60° sector mesh as the injector is symmetrically located in
 127 the middle of the combustion chamber. In this study, the computational grids were firstly created with
 128 different computational cell sizes including 0.6 mm (fine), 0.8 mm (medium), and 0.10 mm (coarse). Figure
 129 2 shows the computational grid at TDC with three different cell sizes. When a computational grid with a
 130 medium cell size of 0.6 mm was used, the results obtained of the in-cylinder mean pressure and rate of heat
 131 release were independent of the number of grid cells. For this reason, the simulations were performed with
 132 a grid of 0.8 mm average cells. The exact number of cells in the mesh was 35240 and 90476 at Top Dead
 133 Center (TDC) and Bottom Dead Center (BDC), respectively.

134 In addition, as can be seen in Figure 2, the crevice above the top piston ring (between the piston and liner)
 135 is resolved and the region under the ring is represented as an additional volume attached to the top ring
 136 crevice. Furthermore, the volumes associated with the valve pockets and pressure transducer crevices are
 137 added to the volume attached to the top ring crevice in order to give the correct compression ratio.

138 Moreover, the ground of the bowl meshed with three continuous layers for a proper calculation of the heat
139 transfer through the piston wall.

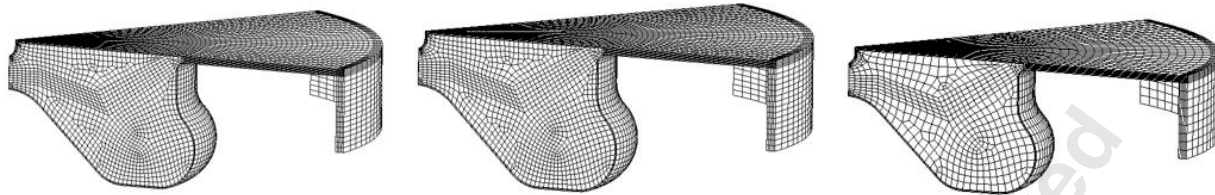


Figure 2. Computational grids at TDC with three different cell sizes

140 A comparison of the predicted and measured in-cylinder pressure and heat release rate is shown in Figure
141 3. The experimental study run at EGR rate equal to 69.6% is used for the validation of the current CFD
142 model.

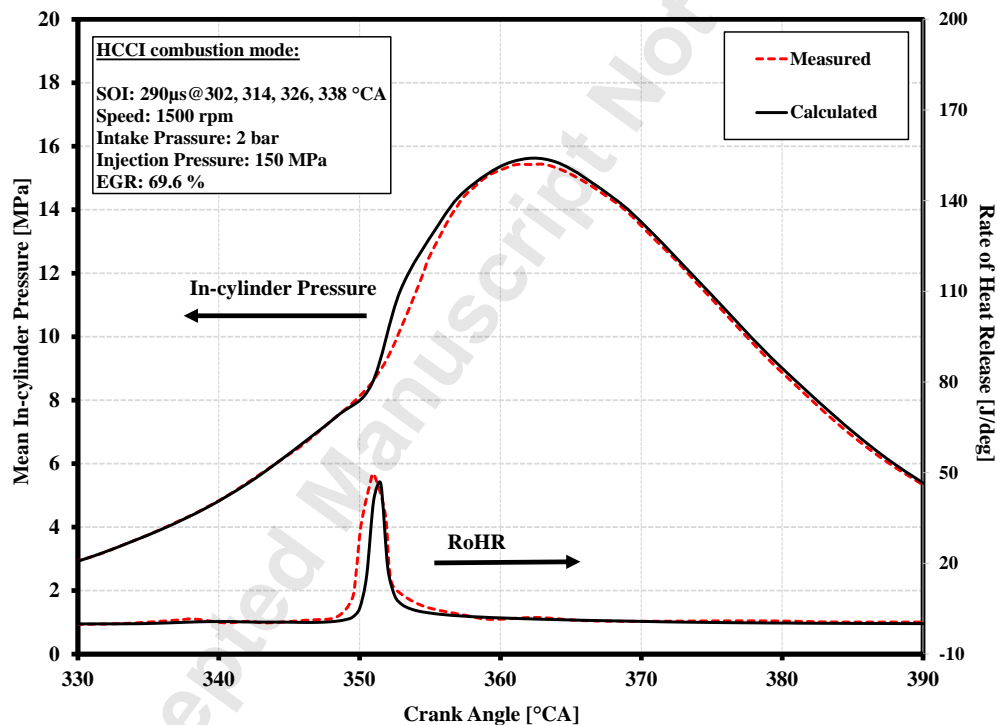


Figure 3. Validation of mean in-cylinder pressure and rate of heat release

143 As can be seen in Figure 3, the present model is seen to perform well, particularly to capture the phasing
144 of the main combustion stage (MSC) under HCCI regime. This confirms that the chemistry scheme
145 employed can be used to simulate the HCCI combustion process. It should be pointed out that in past studies
146 of the authors [21], the current model was analyzed in more detail under other EGR rates and also to

147 evaluate its capabilities to simulate pollutant emissions and a good agreement was obtained for all operating
148 points.

149 Table 4 shows a comparison between experimental data with CFD results to demonstrate the model's
150 capability to predict NO_x, soot and CO emissions. As can be seen in the Table 4, a very good match was
151 achieved between NO_x and soot and CO magnitudes in the simulation.

152 Table 4. Measured and calculated engine-out emissions

Emission	69.6% EGR rate @ 1500 rev/min	
	Measured	Calculated
NO _x [ppm]	13.0	14.0
Soot [g/kWh]	0.000800	0.000850
CO [ppm]	6350	6380

153 4. Oxy-fuel Combustion (OFC)

154 As it is well-known intake temperature is one of the most important engine parameters in controlling the
155 HCCI combustion process. This section describes the CFD investigations performed to analyze the effects
156 of the intake charge temperature on the HCCI OFC characteristics using different CO₂ dilutions. While
157 studying the influence of intake temperature, intake pressure has set to 2.2 bar. Investigations have been
158 conducted using four different CO₂ dilutions ranging from 79% to 85%. Table 5 shows percentages of O₂
159 and CO₂ vol.%, intake charge temperature and the relative O₂-fuel ratio (λ_{O_2}) for each strategy. In
160 Table 2, relative O₂-fuel ratio (λ_{O_2}) is defined using Equation. 1. It must be noted that the oxy-fuel
161 combustion with CO₂ dilution uses a mixture of O₂ and CO₂ rather than air, so instead of "lambda," which
162 represents the actual air-fuel ratio to the stoichiometric air-fuel ratio, we have used the parameter "Lambda
163 O₂" (Relative O₂-fuel ratio), which determines the actual O₂-fuel ratio over O₂-fuel ratio during
164 stoichiometric combustion. Throughout this research, it has been attempted to minimize the cost of oxygen
165 supply by using the lowest relative O₂-fuel ratio (around 1) while maintaining a complete combustion
166 process.

$$167 \quad \text{Lambda}_{\text{O}_2} = \frac{\text{Actual O}_2\text{-fuel ratio}}{\text{O}_2\text{-fuel ratio for stoichiometric combustion}} \quad (3)$$

168 Table 5. Intake charge temperature and relative O₂-fuel ratio for different CO₂ dilutions

Case study (vol.%)	Intake Charge Temperature (°C)	Lambda _{O₂} (Relative O ₂ -fuel ratio)
21% O ₂ + 79% CO ₂	220	1.141
	200	1.189
	180	1.24
	160	1.29
	140	1.36
19% O ₂ + 81% CO ₂	220	1.03
	200	1.07
	180	1.12
	160	1.17
	140	1.23
17% O ₂ + 83% CO ₂	220	0.92
	200	0.96
	180	1.00
	160	1.05
	140	1.10
15% O ₂ + 85% CO ₂	220	0.81
	200	0.84
	180	0.88
	160	0.92
	140	0.96

169 The effect of different CO₂ dilutions on in-cylinder cylinder pressure, and in-cylinder temperature are
 170 shown in Figure 4 and Figure 5, respectively, under a constant intake temperature and intake pressure.

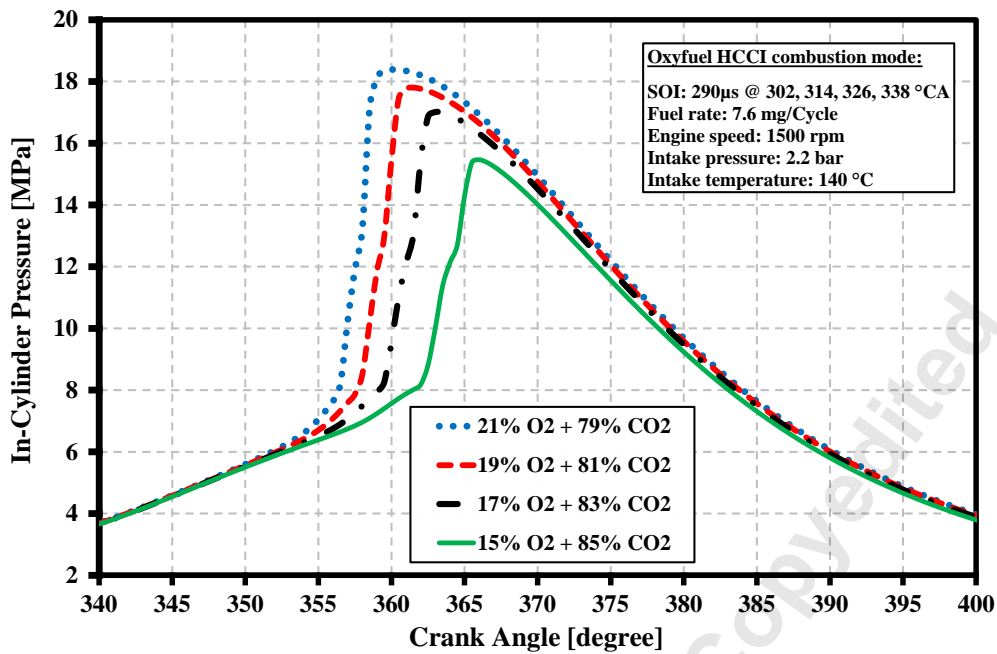


Figure 4. Effect of different CO₂ dilutions on in-cylinder pressure

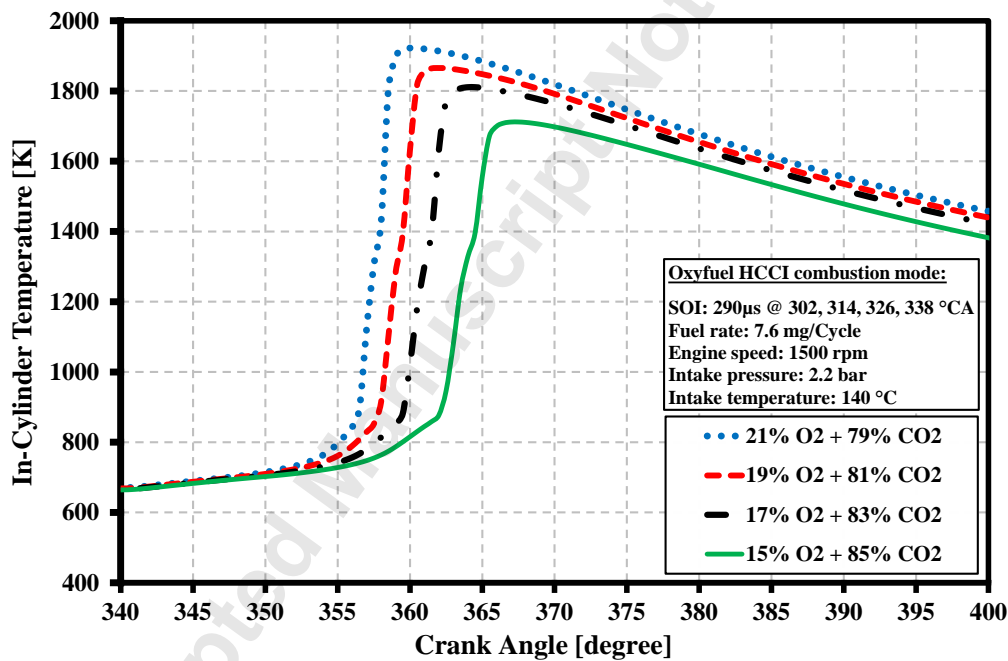


Figure 5. Effect of different CO₂ dilutions on in-cylinder temperature

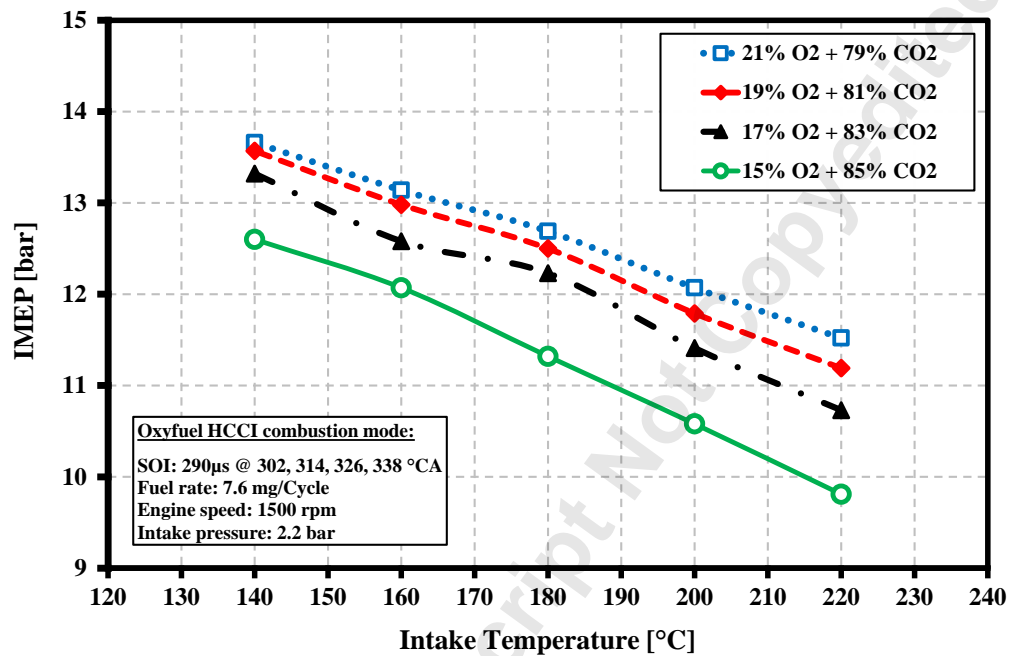
171
172

173
174

175 As illustrated in Figure 4 and Figure 5, the increase of intake-air oxygen content from 15% to 21% results
176 in a significant increase of peak in-cylinder pressure and peak in-cylinder temperature after TDC. In
177 addition, it tends to advance peak pressure location and peak temperature location. Applying oxy-fuel
178 combustion leads to acceleration of the combustion process which results in a shorter ignition delay period.
179 In addition, premixed combustion is minimized while diffusion combustion is maximized. With the heat

180 release rate dramatically increased, it takes a much shorter time to complete the entire heat release process.
181 Subsequently, with such a high heat release rate, the in-cylinder temperature and in-cylinder pressure have
182 increased.

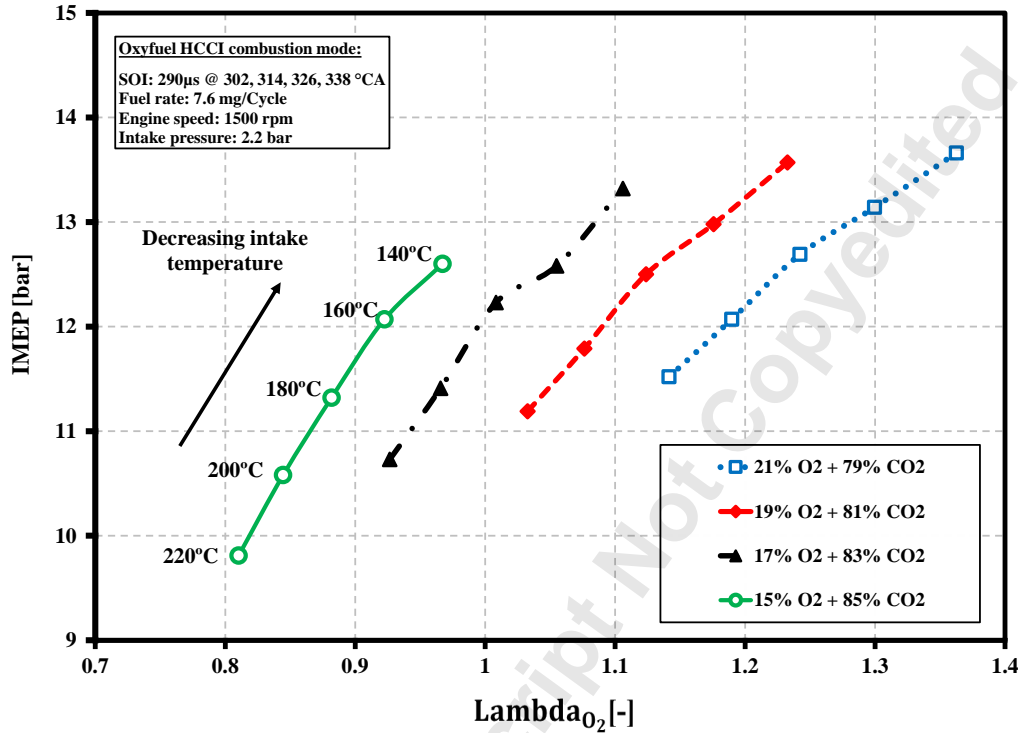
183 The effect of CO₂ dilutions and intake temperature on IMEP is shown in Figure 6.



184 Figure 6. Effect of different CO₂ dilutions and intake temperature on IMEP
185

186 According to Figure 6, maintaining a constant intake pressure while increasing intake temperature from
187 140°C to 220°C decreases IMEP for all diluent cases considered. It can be concluded that increasing intake
188 temperature results in advancing the start of combustion which mainly occurred in the compression stroke.
189 Therefore, some portion of work from the combustion is produced during the compression stroke and it
190 pushes on the piston top as negative work while the piston is still compressing the charge. Then it implies
191 this portion of work has been wasted. Consequently, the IMEP has been negatively affected by increasing
192 the intake temperature. Based on the CFD results, further reduction of intake temperature charge, lower
193 than 140°C, leads to deteriorating the combustion stability and incomplete combustion. Therefore, the
194 implementation of OFC mode using diluent cases must be accompanied by an appropriate intake
195 temperature adjustment.

196 Figure 7 shows the relative O₂-fuel ratio versus IMEP for different CO₂ dilutions. As shown in Figure 7,
197 the IMEP is found to increase when a higher inlet oxygen percentage has applied as represented by
198 increased the relative O₂-fuel ratio while the mass of injected fuel was kept constant.



199 Figure 7. Relative O₂-fuel ratio versus IMEP under different CO₂ dilutions

201 The effect of different diluent strategies and intake temperature on ISFC is shown in Figure 8.

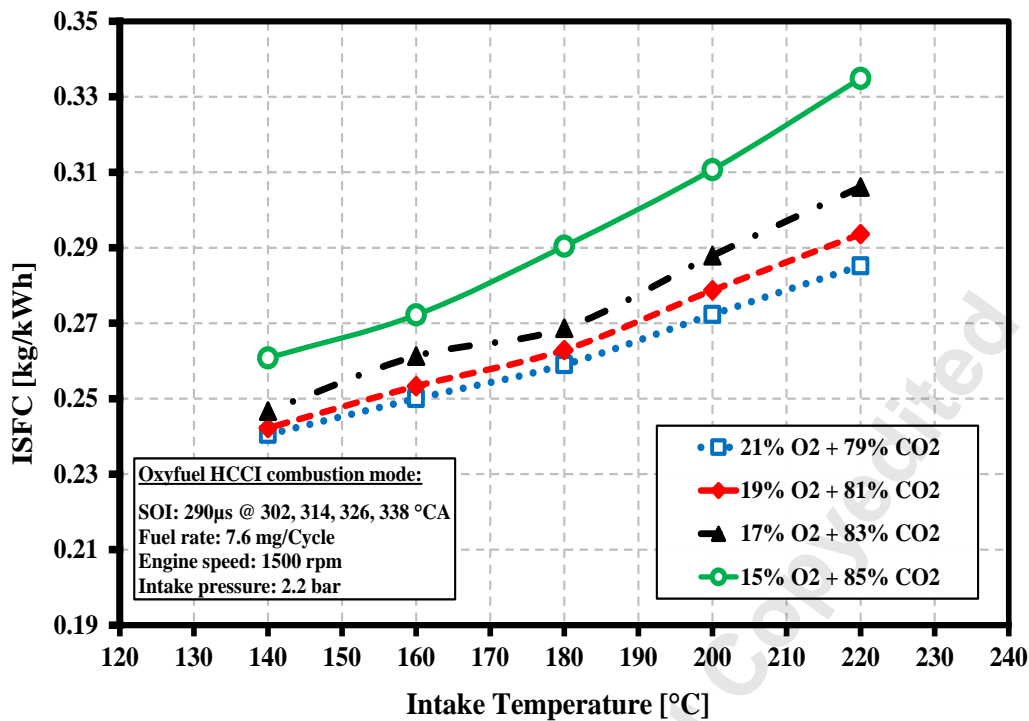


Figure 8. Effect of different CO₂ dilutions and intake temperature on ISFC

As can be seen in Figure 8, the increase of intake temperature under four dilutions results in an increase in ISFC. The ISFC has been increased by 18% when 21% v/v oxygen was applied. It is more pronounced when the intake oxygen fraction is 15%v/v, where the highest ISFC deterioration is around 26%.

Figure 9 shows the relative O₂-fuel ratio versus ISFC under different CO₂ dilutions.

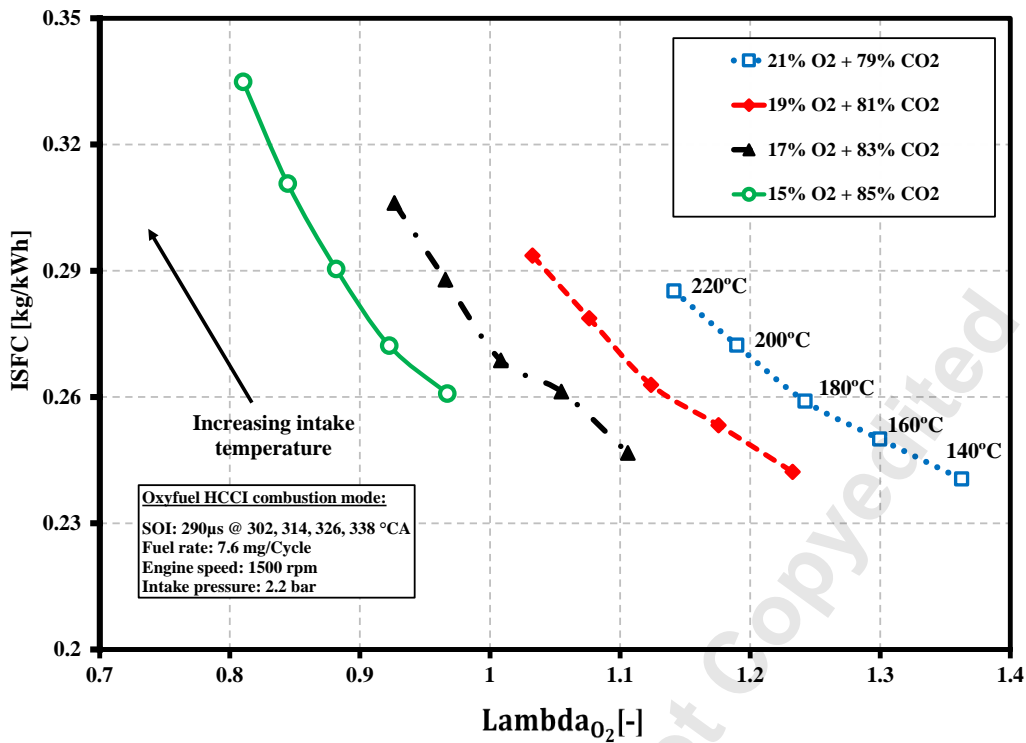
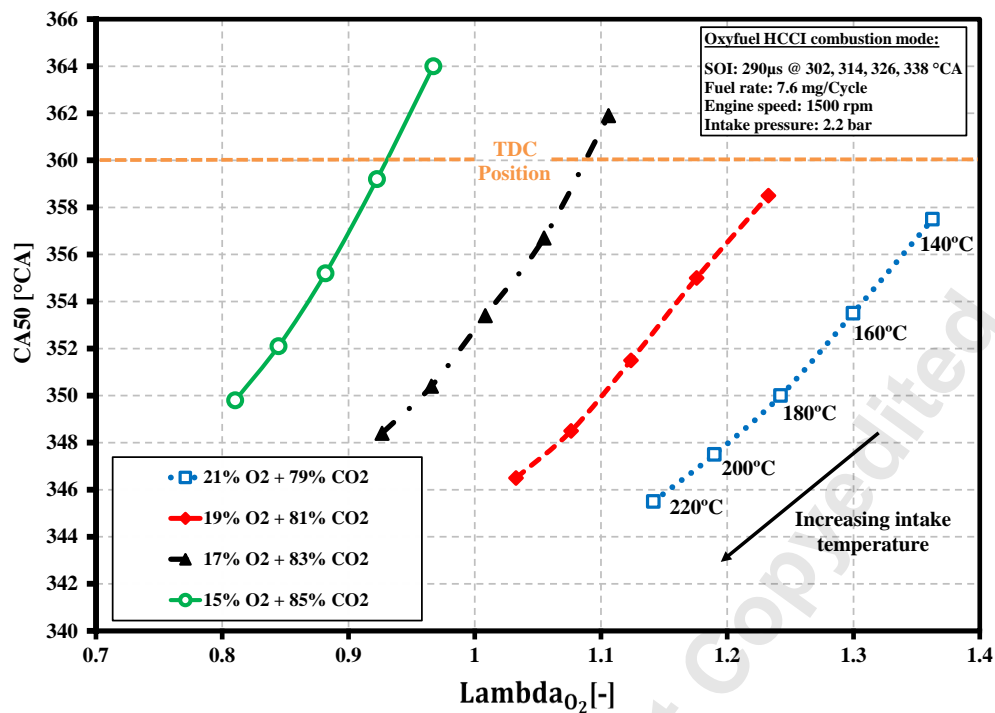


Figure 9. Relative O₂-fuel ratio versus ISFC for different diluent cases

208
209
210

211 As illustrated in Figure 9, by raising the intake charge temperature from 140°C to 220°C and applying 21%
 212 O₂ and 79% CO₂ v/v, ISFC is increased from 0.24 to 0.285 Kg/kWh. In addition, the ISFC has decreased
 213 when a higher inlet O₂ percentage has applied as represented by increased the relative O₂-fuel ratio. By
 214 increasing O₂ percentage from 15%v/v to 21%v/v, the ignition period is shortened and fuel is burned more
 215 rapidly which results in a more complete combustion process and less ISFC while the mass of injected fuel
 216 was kept constant.

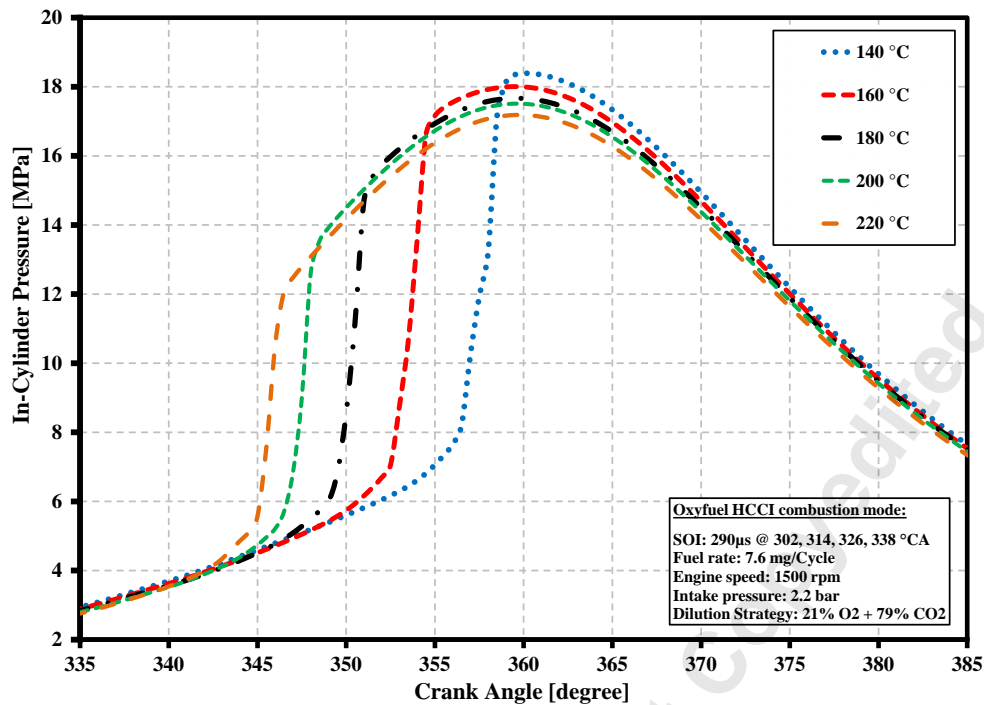
217 Figure 10 shows the effect of oxy-fuel HCCI combustion at different intake temperature charges on CA50.



218
 219 Figure 10. Relative O₂-fuel ratio versus CA50 under different intake temperature charges and CO₂
 220 dilutions

221 According to Figure 10, CA50 timing advances for each dilution strategy as the intake temperature charge
 222 increases between 140°C and 220°C. The earliest CA50 is obtained at 345.5°C when 21% O₂
 223 concentration is applied at 220°C. In addition, at each intake temperature, CA50 retards by decreasing O₂
 224 concentrations from 21 to 15%. The latest CA50 occurred at 4°C after TDC when 15% of intake O₂ is
 225 utilized at 140°C. It can be concluded that decreasing O₂ concentration decreases reaction kinetics, resulting
 226 in more delays in the auto-ignition process.

227 Figure 11 illustrates the in-cylinder pressure at different intake charge temperatures when 21% O₂ and 79%
 228 CO₂ v/v is applied.



229
230
231

Figure 11. Variations of mean in-cylinder pressure under different intake temperatures for the case of $21\%O_2 + 79\%CO_2$

232 Based on Figure 11, the combustion process is advanced with an increase in intake temperature from $140^\circ C$
233 to $220^\circ C$, but the maximum in-cylinder pressure gradually decreases: maximum in-cylinder pressure
234 dropped from 18.34 MPa (under $140^\circ C$ intake temperature) to 17.18 MPa (under $220^\circ C$ intake
235 temperature). The comparison of Figure 11 with Figure 6 illustrates how the advancement of the
236 combustion process has decreased the IMEP and produced much negative work during the compression
237 stroke as a result of the increasing intake charge temperature.

238 An important parameter in the performance of an engine is rate of pressure rise (ROPR), which is a measure
239 of combustion roughness. A comparison of the maximum rate of pressure rise for different diluent cases
240 and intake temperature is shown in Figure 12.

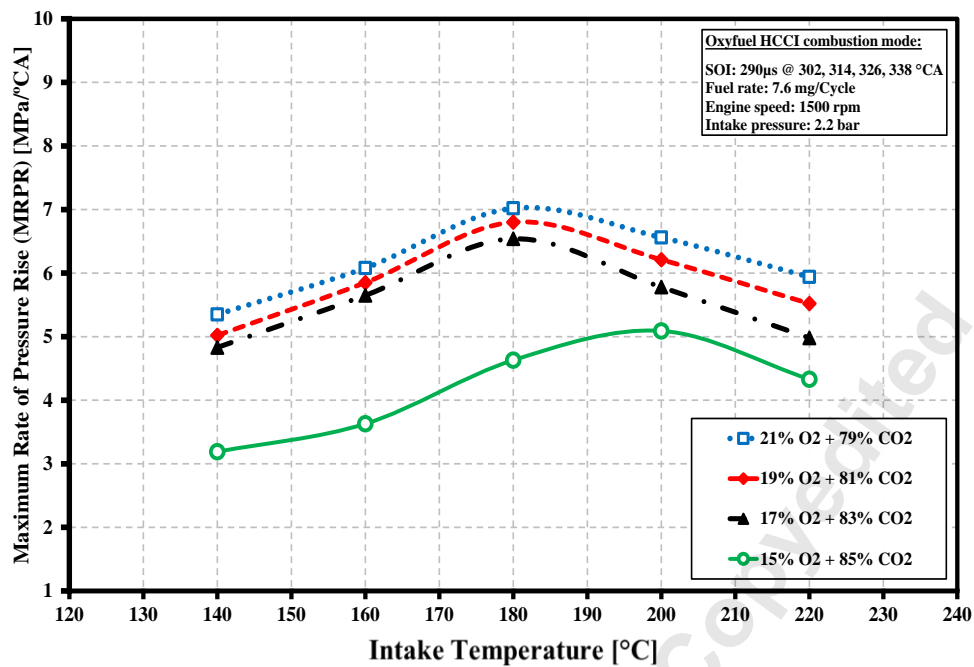


Figure 12. Intake temperature versus maximum rate of pressure rise (MRPR) under different CO₂ dilutions

It has been observed that the MRPR has increased by increasing the concentration of O₂ in the inlet. A higher ROPR indicates a higher proportion of fuel is burned in the premixed combustion phase. When the intake temperature increases from 180°C to 220°C, the MRPR declines with every diluent strategy, possibly due to the decreasing density at higher temperature. Based on these results, the rate of pressure rise in oxy-fuel HCCI combustion increases with intake temperature, then starts to decrease once the intake temperature exceeds 180°C. It may be possible to increase the upper load limit with a lower diluent gas percentage. According to the Figure 12, the maximum MRPR value is 7.02 MPA/°CA which is obtained when 21% of intake O₂ is applied.

Figure 13 illustrates the maximum rate of pressure rise (MRPR) versus the Relative O₂-fuel ratio for various diluent cases.

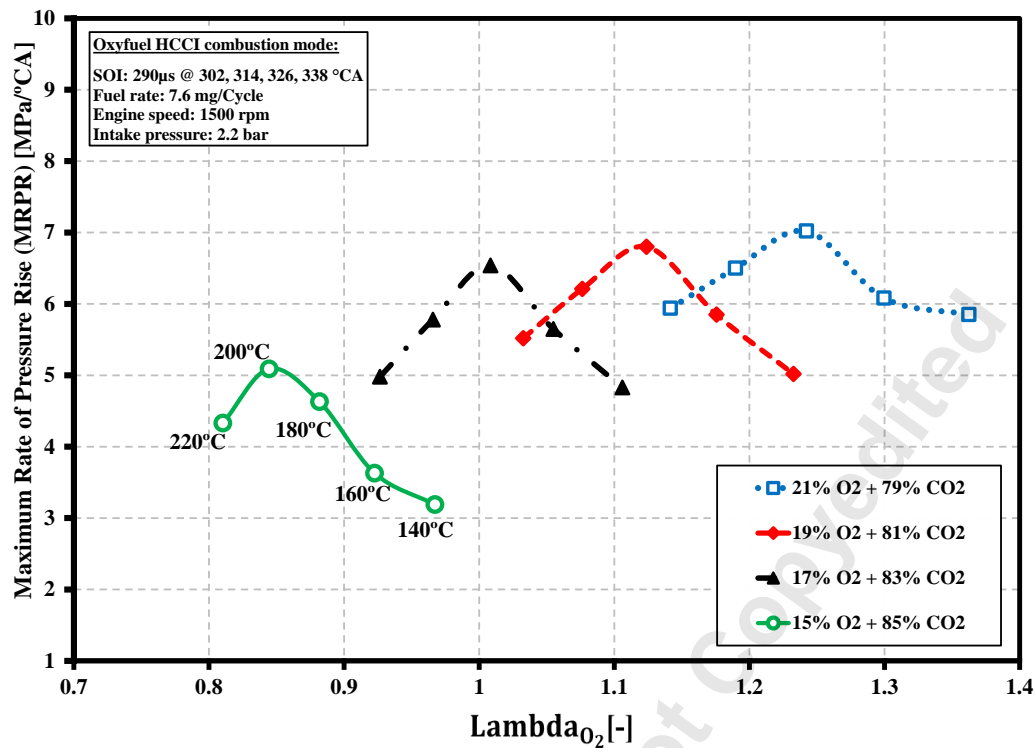
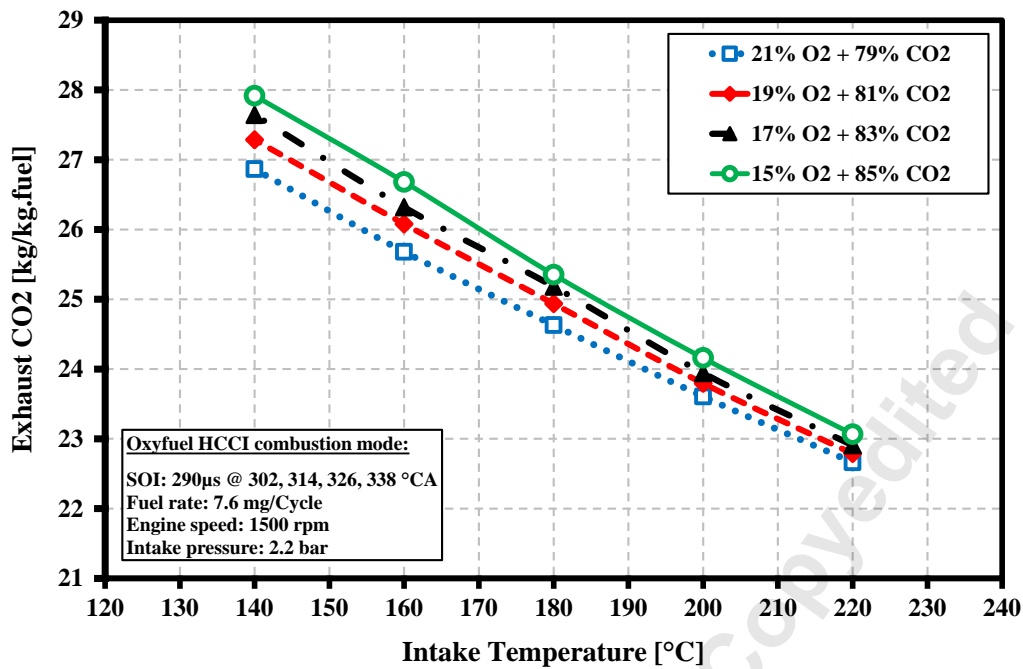


Figure 13. Relative O₂-fuel ratio versus maximum rate of pressure rise (MRPR)

254
255

256 As shown in Figure 13, the MRPR at each intake temperature point has increased as the O₂ concentration
 257 increases between 15 and 21 vol.%. It can be concluded that increasing O₂ concentration results in
 258 increasing the speed of reaction kinetics which leads to an earlier auto-ignition process that results in higher
 259 MRPR. When fuel rate is increased (lower lambda), diluent strategies become more apparent as the
 260 minimum MRPR has achieved by using 15 vol% O₂ in the intake charge. It can be concluded that the
 261 maximum pressure rise rate correlates very strongly with the diluent gas percentage for different intake
 262 charge temperatures. This could result in an increase in HCCI load by increasing the diluent gas
 263 concentration.

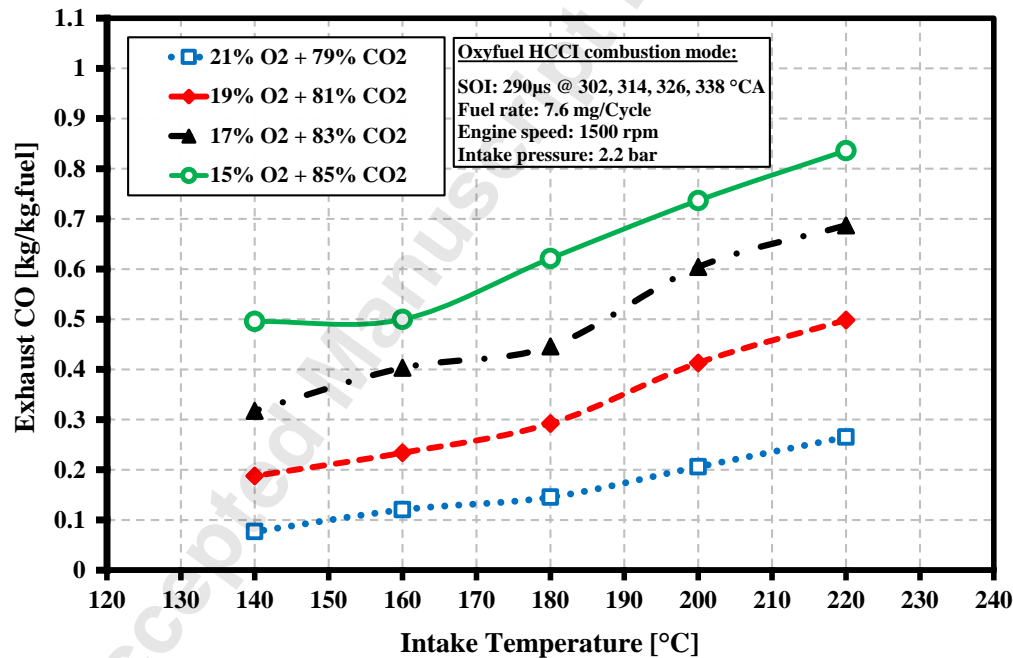
264 Effects of intake temperature on exhaust CO₂ for different diluent strategies is shown in Figure 14. As can
 265 be seen in Figure 14, with increasing the intake temperature from 140°C to 220°C under all diluent
 266 strategies, the amount of exhaust CO₂ have decreased uniformly. This effect can be also attributed to the
 267 increase of burning rate of the injected fuel mass due to higher oxygen availability during the premixed and
 268 diffusion combustion which results in lower exhaust CO₂.



269
270

Figure 14. Effects of intake temperature on exhaust CO₂ for different CO₂ dilutions

271 Figure 15 illustrates the effects of different diluent strategies on exhaust CO emission.



272
273

Figure 15. Effects of intake temperature on exhaust CO for different CO₂ dilutions

274 As shown in Figure 15, the amount of CO emission for all diluent cases was at a low level. The lowest
 275 value of exhaust CO was 0.08 kg/kg-fuel which has obtained at 140°C intake temperature when 15% of
 276 intake CO₂ has been used as a diluent gas. But, when the intake temperature increases up to 220°C the

277 exhaust CO has increased. Moreover, by increasing the intake CO₂ concentration from 79% to 85%, as it
 278 has already been discussed, the in-cylinder pressure has reduced further which leads to more delays in
 279 combustion phasing and a higher amount of CO emissions. In addition, PM emissions from all dilution
 280 cases were extremely low (less than 0.0004 g/kg-fuel) while NO_x emissions were eliminated completely
 281 using HCCI OFC mode.

282 Figure 16 shows the Relative O₂-fuel ratio versus ITE for different diluent cases. As can be seen in Figure
 283 16, by raising the intake charge temperature from 140°C to 220°C and applying 21% O₂ and 79% CO₂ v/v,
 284 ITE is reduced from 34.6% to 29.2% . Moreover, increasing the intake O₂ mass fraction from 15% to 21%
 285 results in an increase in ITE. It can be concluded that, since CO₂ has higher specific heat capacity compared
 286 to O₂, applying the higher percentage of CO₂ dilution will increase the overall specific heat capacity of the
 287 intake charge results in an decrease in in-cylinder pressure during the combustion process which leads to
 288 less ITE.

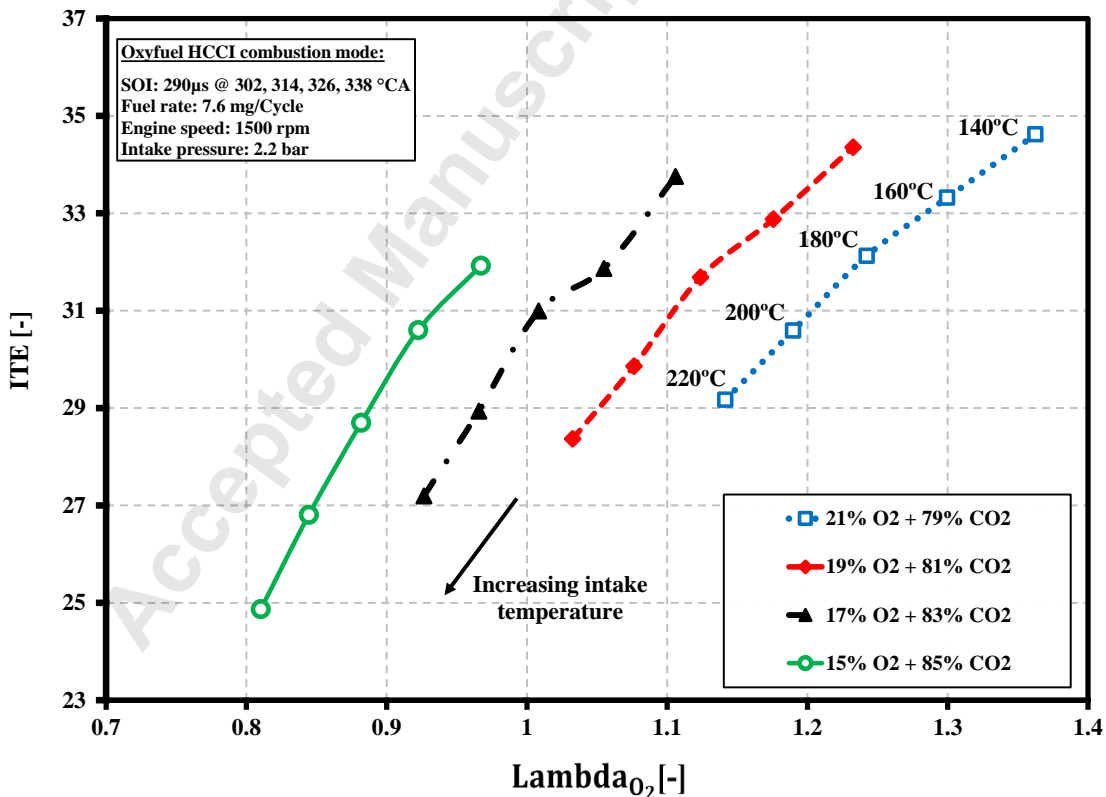


Figure 16. Relative O₂-fuel ratio versus ITE

289
290

291 A comparison of OH radical distributions at 370, 375 and 380 CA degree at two different intake
292 temperatures under the same diluent strategy is shown in Figure 17. Oxidation and soot formation are
293 directly affected by the OH radical, which is one of the most important intermediate species during
294 combustion. Increasing the intake temperature has increased OH formation within the cylinder, as can be
295 observed in Figure 17. Although the amount of OH in both cases is relatively small.

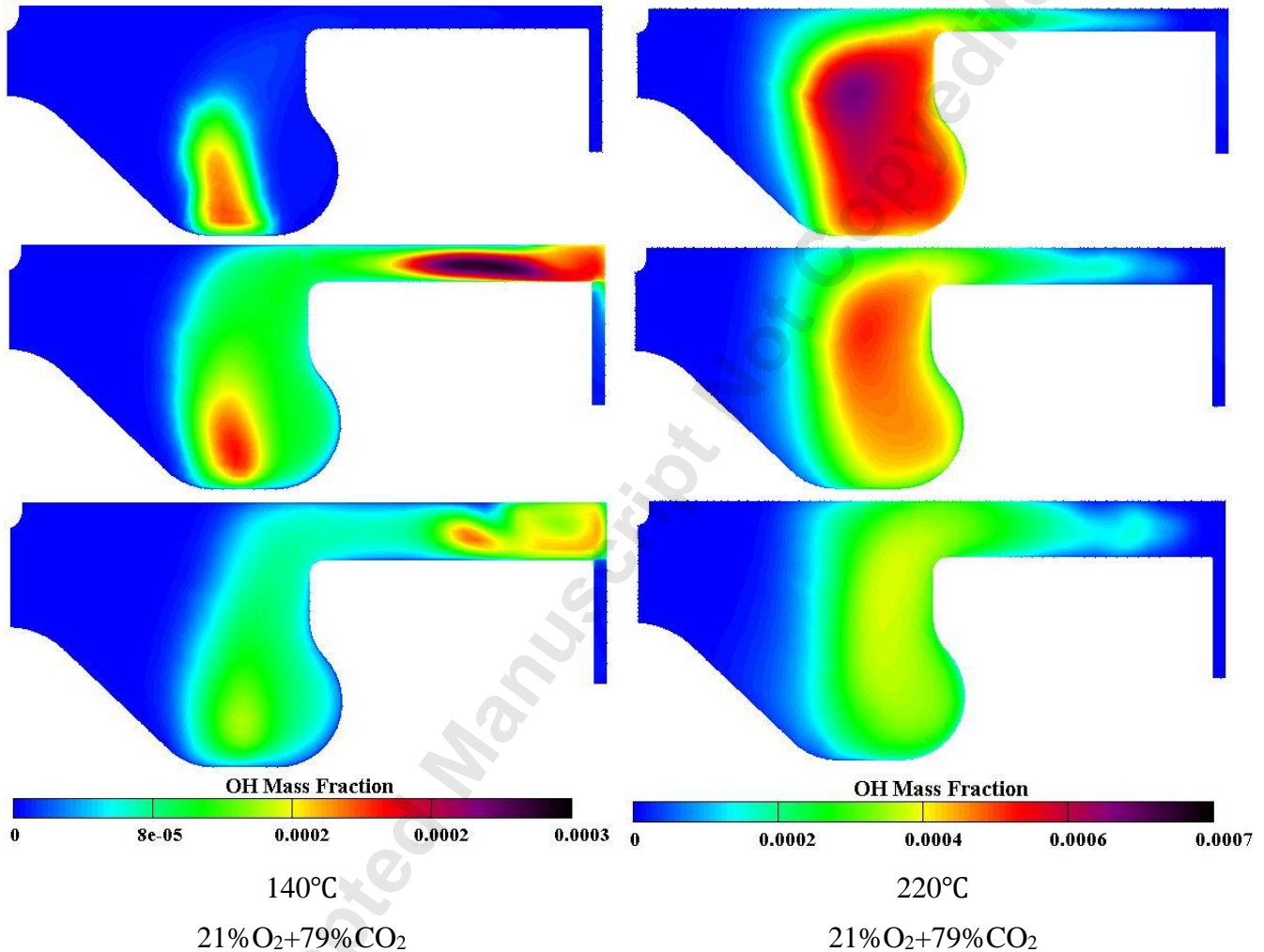


Figure 17. OH distribution at two different intake temperatures under the same diluent strategy

296 Figure 18 shows a comparison of O₂ distributions at 370, 375, and 380 CA degree under the same diluent
297 strategy at two different intake temperatures. As can be seen in Figure 18, the oxygen fraction inside the
298 combustion chamber has decreased with increasing the intake temperature from 140°C to 220°C. At a

299 higher intake temperature, the increase in oxygen consumption results in a shortened ignition time and
300 faster burning of fuel during the combustion process, which leaves less oxygen inside the chamber.
301

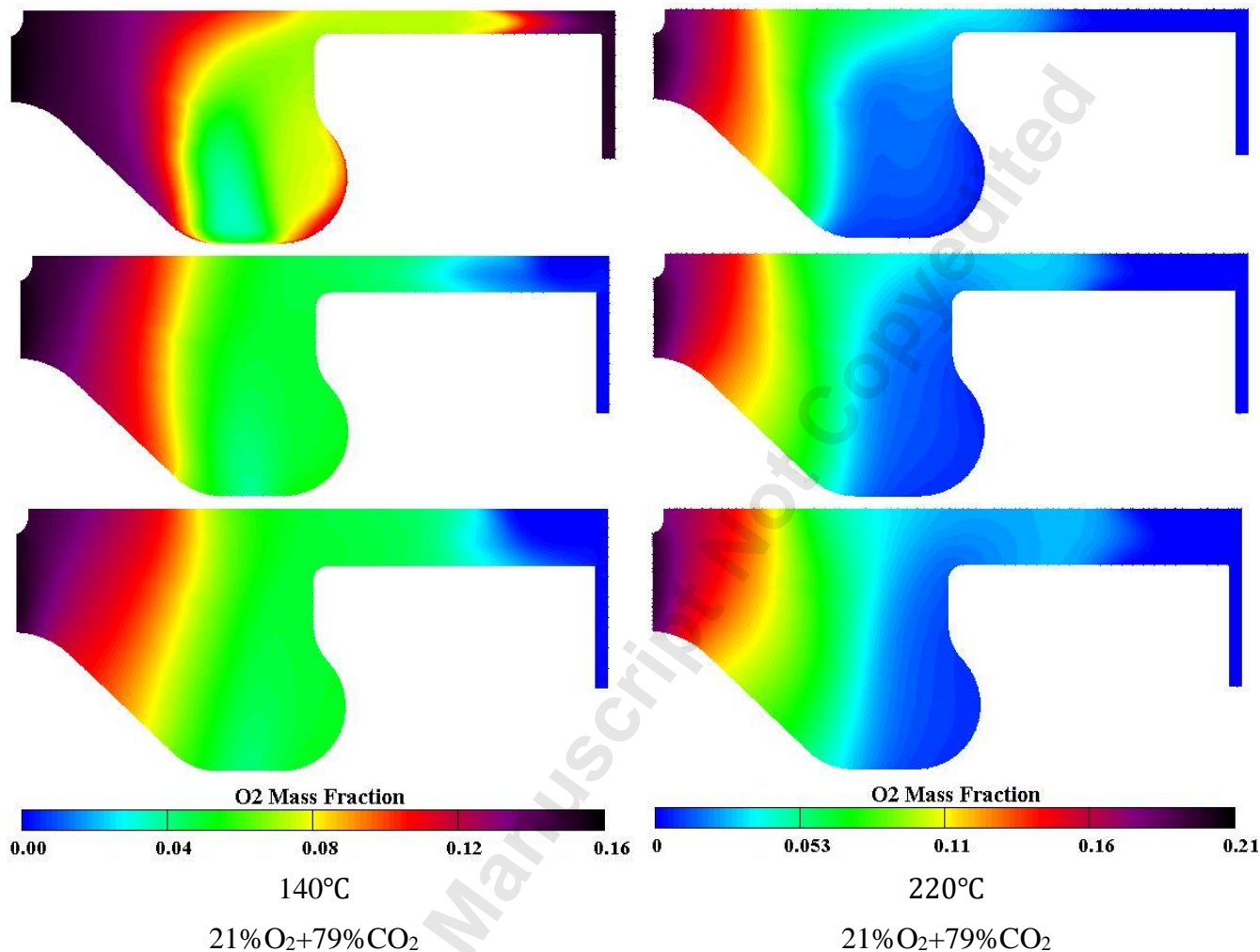


Figure 18. O₂ distribution at two different intake temperatures under the same diluent strategy

302

303 5. Summary and conclusion

304 In this study, a CFD simulation accompanied with the detailed chemistry has been applied to analyze
305 the effects of intake oxygen temperature accompanied with different diluent strategies on the performance
306 characteristics in an HSDI diesel engine under HCCI OFC mode. The following conclusions may be drawn:

- 307 • With OFC technology, PM and CO emissions can be reduced dramatically, while NO_x emissions
308 can be eliminated completely.

- 309 • A proper intake temperature adjustment must accompany the implementation of OFC using CO₂
310 dilution. This study shows that reducing the intake charge temperature to below 140°C over a range
311 of dilution rates adversely affects the combustion stability and results in incomplete combustion.
- 312 • By increasing the concentration of O₂ in the intake charge in a range of 15% to 21% v/v, the reaction
313 kinetics will speed up, leading to an earlier autoignition process with a higher MRPR. For different
314 intake charge temperatures, the maximum pressure rise rate correlates very strongly with the
315 dilution rate. This could potentially allow the HCCI load to be increased by increasing the diluent
316 percentage rate.
- 317 • Under constant diluent rate, by increasing the intake charge temperature from 140°C to 220°C the
318 combustion is advanced which has a negative effect on IMEP as it produced much negative work
319 during the compression stroke. As a result of applying 21% O₂ v/v to the intake charge, the
320 maximum in-cylinder pressure dropped from 18.34 MPa (under 140°C intake temperature) to 17.18
321 MPa (under 220°C intake temperature).
- 322 • A higher proportion of CO₂ dilution will increase the overall specific heat capacity of the intake
323 charge, resulting in a decrease in in-cylinder pressure during the combustion process, which also
324 leads to less ITE.

325 **Acknowledgment**

326 This work is financially supported by the European Regional Development Fund (ERDF) via Interreg
327 North-West Europe (Project No. NWE553). The authors would like to thank the AVL Company for their
328 collaboration in this work to provide the AVL simulation software at JUNIA Graduate School of
329 Engineering, France.

330 **References**

- 331 [1] Tang, Bao-Jun, Yang-Yang Guo, Biying Yu, and LD Danny Harvey. "Pathways for decarbonizing
332 China's building sector under global warming thresholds." *Applied Energy* 298 (2021): 117213.
- 333 [2] IPCC, Climate Change. "Contribution of working group II to the fifth assessment report of the
334 Intergovernmental Panel on Climate Change." *Mitigation of climate change* 1454 (2014).
- 335 [3] Mobasheri, Raouf, and Zhijun Peng. The development and application of homogeneity factor on DI
336 diesel engine combustion and emissions. No. 2013-01-0880. SAE Technical Paper, 2013.
- 337 [4] Verichev, Konstantin, Montserrat Zamorano, and Manuel Carpio. "Effects of climate change on
338 variations in climatic zones and heating energy consumption of residential buildings in the southern
339 Chile." *Energy and Buildings* 215 (2020): 109874.
- 340 [5] García, Antonio, Javier Monsalve-Serrano, Rafael Lago Sari, and Shashwat Tripathi. "Life cycle CO₂
341 footprint reduction comparison of hybrid and electric buses for bus transit networks." *Applied Energy*
342 308 (2022): 118354.
- 343 [6] Pelletier, Chloé, Yann Rogaume, Léa Dieckhoff, Guillaume Bardeau, Marie-Noëlle Pons, and
344 Anthony Dufour. "Effect of combustion technology and biogenic CO₂ impact factor on global
345 warming potential of wood-to-heat chains." *Applied Energy* 235 (2019): 1381-1388.
- 346 [7] Huang, Weilong, Wenying Chen, and Gabriel Anandarajah. "The role of technology diffusion in a
347 decarbonizing world to limit global warming to well below 2 C: An assessment with application of
348 Global TIMES model." *Applied energy* 208 (2017): 291-301.
- 349 [8] Li, Xiang, Yiqiang Pei, Dayou Li, Tahmina Ajmal, Abdel Aitouche, Raouf Mobasheri, and Zhijun
350 Peng. "Implementation of oxy-fuel combustion (OFC) technology in a gasoline direct injection (GDI)
351 engine fueled with gasoline-ethanol blends." *ACS omega* 6, no. 44 (2021): 29394-29402.
- 352 [9] Anwar, M. N., A. Fayyaz, N. F. Sohail, M. F. Khokhar, M. Baqar, W. D. Khan, K. Rasool, M. Rehan,
353 and A. S. Nizami. "CO₂ capture and storage: A way forward for sustainable environment." *Journal of
354 environmental management* 226 (2018): 131-144.

- 355 [10] Wang, Chang'an, Xiaoming Zhang, Yinhe Liu, and Defu Che. "Pyrolysis and combustion
356 characteristics of coals in oxyfuel combustion." *Applied Energy* 97 (2012): 264-273.
- 357 [11] Simpson, Adam P., and A. J. Simon. "Second law comparison of oxy-fuel combustion and post-
358 combustion carbon dioxide separation." *Energy Conversion and Management* 48, no. 11 (2007): 3034-
359 3045.
- 360 [12] Pei, Xiaohui, Boshu He, Linbo Yan, Chaojun Wang, Weining Song, and Jingge Song. "Process
361 simulation of oxy-fuel combustion for a 300 MW pulverized coal-fired power plant using Aspen Plus."
362 *Energy Conversion and Management* 76 (2013): 581-587.
- 363 [13] Hanak, Dawid P., Dante Powell, and Vasilije Manovic. "Techno-economic analysis of oxy-
364 combustion coal-fired power plant with cryogenic oxygen storage." *Applied Energy* 191 (2017): 193-
365 203.
- 366 [14] Wei, Xiaoyu, Vasilije Manovic, and Dawid P. Hanak. "Techno-economic assessment of coal-or
367 biomass-fired oxy-combustion power plants with supercritical carbon dioxide cycle." *Energy*
368 *Conversion and Management* 221 (2020): 113143.
- 369 [15] Biyiklioglu, Onur, and Mustafa Ertunc Tat. "Tribological assessment of NiCr, Al₂O₃/TiO₂, and
370 Cr₃C₂/NiCr coatings applied on a cylinder liner of a heavy-duty diesel engine." *International Journal*
371 *of Engine Research* 22, no. 7 (2021): 2267-2280.
- 372 [16] Escudero, Ana I., Sergio Espatolero, and Luis M. Romeo. "Oxy-combustion power plant integration
373 in an oil refinery to reduce CO₂ emissions." *International Journal of Greenhouse Gas Control* 45
374 (2016): 118-129.
- 375 [17] European Environment Agency. accessed April 29, 2021. [https://www.eea.europa.eu/ims/greenhouse-
376 gas-emissions-from-transport](https://www.eea.europa.eu/ims/greenhouse-gas-emissions-from-transport)
- 377 [18] Decan, Gilles, Stijn Broekaert, Tommaso Lucchini, Gianluca D'Errico, Jan Vierendeels, and Sebastian
378 Verhelst. "Evaluation of wall heat flux calculation methods for CFD simulations of an internal
379 combustion engine under both motored and HCCI operation." *Applied energy* 232 (2018): 451-461.

- 380 [19] Metz, Bert, Ogunlade R. Davidson, Peter R. Bosch, Rutu Dave, and Leo A. Meyer. "Contribution of
381 working group III to the fourth assessment report of the intergovernmental panel on climate change."
382 (2007).
- 383 [20] The Interreg North-West Europe. River - Non-carbon River Boat Powered by combustion Engines.
384 [https://www.nweurope.eu/projects/project-search/river-non-carbon-river-boat-powered-by-](https://www.nweurope.eu/projects/project-search/river-non-carbon-river-boat-powered-by-combustion-engines/)
385 [combustion-engines/](https://www.nweurope.eu/projects/project-search/river-non-carbon-river-boat-powered-by-combustion-engines/)
- 386 [21] Mobasheri, Raouf, Abdel Aitouche, Zhijun Peng, and Xiang Li. "A numerical study of the effects of
387 oxy-fuel combustion under homogeneous charge compression ignition regime." *International Journal*
388 *of Engine Research* 23, no. 4 (2022): 649-660.
- 389 [22] Zheng, Ge, and Zhijun Peng. "Life Cycle Assessment (LCA) of BEV's environmental benefits for
390 meeting the challenge of ICExit (Internal Combustion Engine Exit)." *Energy Reports* 7 (2021): 1203-
391 1216.
- 392 [23] Li, Xiang, Zhijun Peng, Yiqiang Pei, Tahmina Ajmal, Khaqan-Jim Rana, Abdel Aitouche, and Raouf
393 Mobasheri. "Oxy-fuel combustion for carbon capture and storage in internal combustion engines—A
394 review." *International Journal of Energy Research* 46, no. 2 (2022): 505-522.
- 395 [24] Jordal, Kristin, Marie Anheden, Jinying Yan, and Lars Strömberg. "Oxyfuel combustion for coal-fired
396 power generation with CO2 capture—opportunities and challenges." *Greenhouse Gas Control*
397 *Technologies* 7 (2005): 201-209.
- 398 [25] Buhre, Bart JP, Liza K. Elliott, C. D. Sheng, Rajender P. Gupta, and Terry F. Wall. "Oxy-fuel
399 combustion technology for coal-fired power generation." *Progress in energy and combustion science*
400 31, no. 4 (2005): 283-307.
- 401 [26] Osman, Azmi. "Feasibility study of a novel combustion cycle involving oxygen and water." *SAE*
402 *technical paper* (2009): 01-2808.

- 403 [27] Kang, Zhe, Zhijun Wu, Zhehao Zhang, Jun Deng, Zongjie Hu, and Liguang Li. "Study of the
404 combustion characteristics of a HCCI engine coupled with oxy-fuel combustion mode." SAE
405 International Journal of Engines 10, no. 3 (2017): 908-916.
- 406 [28] Li, Xiang, Zhijun Peng, Tahmina Ajmal, Abdel Aitouche, Raouf Mobasher, Yiqiang Pei, Bo Gao,
407 and Matthias Wellers. "A feasibility study of implementation of oxy-fuel combustion on a practical
408 diesel engine at the economical oxygen-fuel ratios by computer simulation." Advances in Mechanical
409 Engineering 12, no. 12 (2020): 1687814020980182.
- 410 [29] Yu, Xiao, Zhijun Wu, Lezhong Fu, Jun Deng, Zongjie Hu, and Liguang Li. Study of combustion
411 characteristics of a quasi internal combustion rankine cycle engine. No. 2013-01-2698. SAE Technical
412 Paper, 2013.
- 413 [30] Bouillon, Pierre-Antoine, Sophie Hennes, and Céline Mahieux. "ECO2: Post-combustion or Oxyfuel—
414 A comparison between coal power plants with integrated CO2 capture." Energy Procedia 1, no. 1
415 (2009): 4015-4022.
- 416 [31] Telli, Giovanni Dambros, Carlos Roberto Altafini, Carlos Alberto Costa, Josimar Souza Rosa, Mario
417 Eduardo Martins, and Luiz Alberto Oliveira Rocha. "A comprehensive review of homogeneous charge
418 compression ignition (HCCI) engines: Advantages, challenges and evolution." (2021).
- 419 [32] ICE Physics & Chemistry, AVL FIRE user manual.2021.1, 2021.
- 420 [33] Wang, Hu, Rolf Deneys Reitz, Mingfa Yao, Binbin Yang, Qi Jiao, and Lu Qiu. "Development of an
421 n-heptane-n-butanol-PAH mechanism and its application for combustion and soot prediction."
422 Combustion and Flame 160, no. 3 (2013): 504-519.
- 423 [34] Mobasher, Raouf, and Mahdi Seddiq. Effects of diesel injection parameters in a heavy duty iso-
424 butanol/diesel reactivity controlled compression ignition (RCCI) engine. No. 2018-01-0197. SAE
425 Technical Paper, 2018.
- 426 [35] Mobasher, Raouf, Abdel Aitouche, Zhijun Peng, and Xiang Li. Influence of oxy-fuel combustion on
427 engine operating conditions and combustion characteristics in a High Speed Direct Injection (HSDI)

- 428 diesel engine under Homogenous Charge Compression Ignition (HCCI) mode. No. 2020-01-1138.
429 SAE Technical Paper, 2020.
- 430 [36] Mobasheri, Raouf, Abdel Aitouche, Xiang Li, and Zhijun Peng. Analysis of the Influence of Inlet
431 Temperature on Oxy-Fuel Combustion in an HSDI Diesel Engine. No. 2022-37-0003. SAE Technical
432 Paper, 2022.

Accepted Manuscript Not Copyedited